Desalination and Water Treatment
www.deswater.com
doi: 10.5004/dwt.2022.28466

260 (2022) 139–147
June

Chloride ions adsorption behavior on CaMnFe-LDHs and solidification performance of chloride ions on cement slurry blocks containing CaMnFe-LDHs

Youwen Xu[a,*], Weiyou Wang[b], Luming Liang[a], Shiyu Zhang[a]

[a]*College of Civil Engineering, Xi'an Traffic Engineering Institute, Xi'an 710300, China, email: shi8953357@163.com (Y. Xu)*
[b]*Qingyang Yuan Tong Highway Engineering Co., Ltd., Qingyang 745000, China*

Received 5 December 2021; Accepted 22 March 2022

ABSTRACT

To improve the resistance of concrete structures to chloride ion attack, CaMnFe-LDHs (layered double hydroxides) were prepared by co-precipitation method. The CaMnFe-LDHs was used to adsorb Cl^- from aqueous solutions and cement slurry block containing CaMnFe-LDHs was applied to solidify Cl^-. Adsorption experiments showed that the Cl^- adsorption process on CaMnFe-LDHs was in accordance with the pseudo-second-order model and Langmuir model. The Cl^- maximum adsorption capacity on CaMnFe-LDHs could reach 144.01 mg/g. The mechanism of Cl^- removal by CaMnFe-LDHs involved adsorption of O-containing groups and ion exchange. Solidification experiments showed that the cement slurry block with CaMnFe-LDHs had significantly improved its Cl^- solidification ability compared to ordinary cement slurry block. At an admixture rate of 20:100 and curing age of 28 d, the Cl^- solidification amount (155.74 mg) and Cl^- adsorption capacity (56.15 mg/g) on cement slurry block reached the optimum value. The results indicated that CaMnFe-LDHs can effectively prevent the attack of Cl^- on cement slurry block.

Keywords: Layered double hydroxides; Chloride ion; Adsorption; Cement slurry block; Solidification

1. Introduction

Since entering the 21st century, the marine infrastructure construction investment has increased, and reinforced concrete structures are widely used in marine terminals, ports, cross-sea bridges and offshore exploration platforms and other projects [1,2]. And these engineering structures are long-term in the seawater environment, erosion by a large number of chloride ions, will lead to structural durability deficiencies. Therefore, the study of chloride salt erosion in concrete, especially how to mitigate the chloride salt erosion is still the focus of the concrete durability research field [3].

Hydrotalcite-based intercalation materials, also known as layered double hydroxides (LDHs), had a strong interlayer anion exchange capacity [4,5]. One of the effects of LDHs on the durability of concrete materials was to improve resistance to chloride attack, and research had focused on both their adsorption of chloride ions and slowing down chloride ion penetration [6–8]. Adsorption methods are widely used for the removal of organic and inorganic contaminants from aqueous solutions [9–11]. The simplicity and efficiency of adsorption methods have attracted the attention of researchers worldwide [12–14]. Tang et al. [15] incorporated CaMg-LDHs into cement and studied its mechanical properties and chloride ion curing properties. The results showed that the concrete mixed with CaMg-LDHs had efficient, rapid and stable chloride ion exchange behavior and curing ability, and the optimal amount of CaMg-LDHs in cement was 3%, which can significantly improve the curing chloride ion ability of cement. Yoon et al. [16] showed that the Cl^- curing capacity

* Corresponding author.

of MgAl-LDHs was 153 mg/g, and further demonstrated that MgAl-LDHs can significantly enhance the curing capacity of cementitious materials against Cl^-. Ma et al. [17] showed that MgAl-LDHs can significantly enhance the Cl^- penetration resistance of concrete materials and attributed the reason to adsorption of Cl^-. It had also been confirmed that MgAl-LDHs, MgNiAl-LDHs and composites of MgAl-LDHs incorporated into cement slurry block were effective in curing Cl^- [18,19].

In this paper, CaMnFe-LDHs were prepared by co-precipitation method and used for the adsorption and immobilization of Cl^-. The main objectives of this paper are to: (1) investigate the adsorption performance of CaMnFe-LDHs on Cl^-, and (2) explore the Cl^- solidification performance of cement slurry block with Mg-Al-CLDHs admixture ratios.

2. Materials and methods

2.1. Reagents

$Ca(NO_3)_2{\cdot}4H_2O$, $Mn(NO_3)_2{\cdot}4H_2O$, $Fe(NO_3)_3{\cdot}9H_2O$ and NaCl were analytical reagent (AR) and were purchased from Sinopharm Chemical Reagent Co., Ltd., (Shanghai, China). The purity of all reagents is over 99.7%. The experimental water was deionized water (DW).

2.2. Preparation of materials

CaMnFe-LDHs were prepared by co-precipitation method: 0.05 mol $Ca(NO_3)_2{\cdot}4H_2O$, 0.025 mol $Mn(NO_3)_2{\cdot}4H_2O$ and 0.025 mol $Fe(NO_3)_3{\cdot}9H_2O$ were dissolved in 100 mL DW, and the solution pH was adjusted to 10 using 1 mol/L NaOH. Then, the mixed solution was transferred to a 500 mL three-neck flask. After the reaction was completed, the flask was sealed with plastic film and placed in a water bath at 60°C for 24 h. After the reaction was completed, the solid was filtered by centrifugation and washed with DW for several times. The washed solid was dried under vacuum for 12 h to obtain CaMnFe-LDHs.

2.3. Adsorption experiments

A certain amount of CaMnFe-LDHs and 50 mL of Cl^- solution were mixed, and the initial pH of the solution was adjusted by 0.1 mol/L of HCl or NaOH. Subsequently, the mixed solution placed in a constant temperature oscillator at 150 rpm for a reaction period to investigate the effects of the dosage (0.1~3 g/L), the initial pH (2~10), the reaction time (10~600 min), temperature (15°C~50°C) and the initial Cl^- concentration (50~1,000 mg/L) on the Cl^- adsorption by CaMnFe-LDHs. After the adsorption was completed, 10 mL solution was centrifuged for 10 min. The Cl^- concentration of the solution was measured by a chloride ion selective electrode (The chloride ion selective electrode determined the Cl^- concentration by the ion selective electrode (ISE) method. The measurement mechanism was that the ISE was converted into a certain potential according to the concentration of chloride ions to obtain the concentration of chloride ions in solution), and the NO_3^- concentration of the filtrate was determined by the phenol-disulfonic acid colorimetric method. Finally, the removal efficiency [Eq. (1)] and adsorption capacity [Eq. (2)] were calculated as follows:

$$R = \frac{C_0 - C_e}{C_0} \times 100\% \tag{1}$$

$$Q = \frac{\left(C_0 - C_e\right) \times V}{m} \tag{2}$$

where R is the Cl^- removal efficiency, %; C_0 is the initial concentration, mg/L; C_e is the remaining Cl^- concentration in the solution after adsorption equilibrium, mg/L; Q_e is the adsorption capacity, mg/g; V is the volume of the solution, mL; m is the mass of the adsorbent, mg.

2.4. Solidification experiments

The CaMnFe-LDHs with certain ratios (0:100, 5:100, 10:100, 15:100, 20:100 and 25:100) were mixed into cement as cement admixture, and cement slurry was mixed with DW to prepare cement slurry block (size: 20 mm × 20 mm × 20 mm). The curing age of cement slurry block were set to 3, 7 and 27 d. The group with a mixing ratio of 0:100 was identified as the control check group (CK) and the rest groups were the experimental group (EG). According to the ratios (5:100, 10:100, 15:100, 20:100 and 25:100), the experimental groups were recorded as EG-1, EG-2, EG-3, EG-4, and EG-5, respectively.

The cement slurry blocks were placed in 1 mol/L Cl^- solution (50 mL) to soak for 28 d. The Cl^- concentration in the aqueous solution after soaking was measured by a Cl^- selective electrode. The reduction of Cl^- before and after soaking was regarded as solidification amount on cement slurry block. The Cl^- solidification amount by CaMnFe-LDHs in cement slurry blocks (Cl^- amount in EG soaking solution after solidification – Cl^- amount in CK soaking solution after solidification) and the Cl^- adsorption capacity on CaMnFe-LDHs in cement slurry blocks (solidification amount/CaMnFe-LDHs admixture) were calculated as follows [20].

2.5. Structural characterization of the materials

CaMnFe-LDHs crystalline structure was analyzed by X-ray powder diffractometer (XRD, D8, Bruker, Germany). The surface morphological features and surface elements were analyzed by scanning electron microscope with energy-dispersive X-ray spectrometer (SEM-EDS, SUPRA40, Zeiss, Germany). The surface functional groups were analyzed by Fourier-transform infrared spectrometer (FTIR, Nicolet-460, Thermo Fisher, USA). The specific surface area and pore size analysis were analyzed by specific surface area analyzer (BET, Tristar II Plus 2.02, Micromeritics, USA). The zeta potential analyzer (Nano-ZS90, Malvern, England) was used to analyze the surface potential changes at different pH and to calculate zero potential points (pH_{pzc}).

3. Results and discussion

3.1. Characterization analysis

As shown in Fig. 1, the surface morphology of CaMnFe-LDHs was magnified by 30,000 times. Before adsorption (Fig. 1a), the surface of CaMnFe-LDHs was rough and loose,

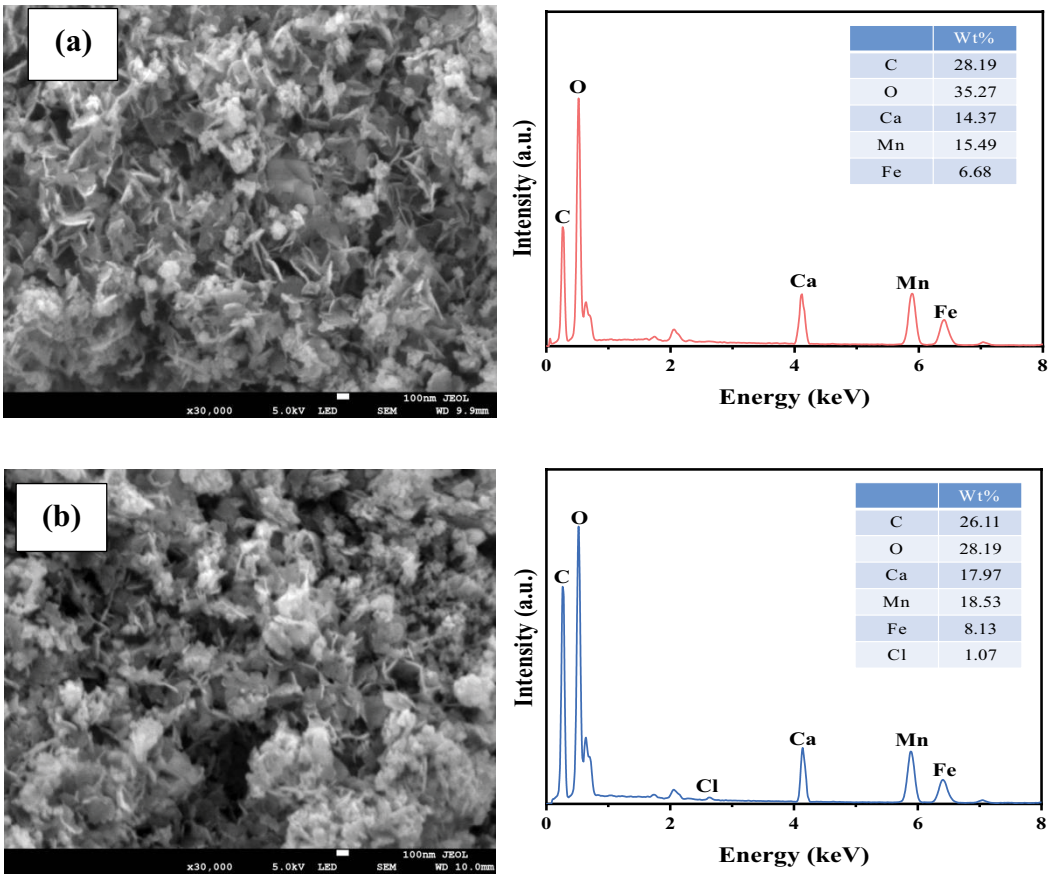

Fig. 1. SEM-EDS images of Cl^- removal by CaMnFe-LDHs before (a) and after (b).

showing irregular lamellar structure with sharp angles, which was typical structure of LDHs. After Cl^- adsorption (Fig. 1b), CaMnFe-LDHs exhibited interlayer aggregation and collapse, but the basic structure remained unchanged. The EDS analysis before and after adsorption manifested that Cl^- was successfully adsorbed by CaMnFe-LDHs.

The N_2 adsorption–desorption isotherms and pore-size distribution of CaMnFe-LDHs are dispalyed in Fig. 2a and b, respectively. The N_2 adsorption–desorption isotherm can be classified as type IV isotherm [11,21,22]. Additionally, the pore-size distribution confirmed that the pore size of CaMnFe-LDHs was in the range of 2~50 nm, indicating that CaMnFe-LDHs was a mesoporous material [21,23,24]. Simultaneously, the specific surface area and pore size were calculated to be 436.28 m^2/g and 2.39 nm, respectively.

FTIR characterization of the CaMnFe-LDHs was performed as shown in Fig. 2c. The strong and broad diffraction peak at 3,420 cm^{-1} was mainly due to the –OH in CaMnFe-LDHs. The spectrum of CaMnFe-LDHs shown an absorption band near 1,630 cm^{-1}, which may be the superposition peak of interlayer water molecules with C=O functional groups [21,25]. The obvious shoulder peak at 1,390 cm^{-1} indicated the highly symmetric and well-arranged interlayer NO_3^-, which proved the presence of NO_3^- in the interlayer [26]. The peak at 559 cm^{-1} in both samples was mainly due to laminar metal lattice stretching vibrations (e.g., Ca–O, Mn–O and Fe–O) [27,28].

The XRD analysis of CaMnFe-LDHs material were displayed in Fig. 2c. The presence of distinct diffraction peaks at 2θ of 11.54°, 23.32°, 33.03°, 57.16° and 58.66°, corresponding to (003), (006), (009), (110) and (113) diffraction crystal planes, respectively, were typical characteristic peaks of LDHs, which also indicated the successful preparation of CaMnFe-LDHs [19,21,29–32]. Crystal planes (003), (006) and (009) corresponded to 2θ with multiplicative relationship and sharp and pointed diffraction peaks, confirming that the synthesized CaMnFe-LDHs had typical characteristic peaks of LDHs [31].

3.2. Adsorption kinetics

The effect of reaction time (10~600 min) on the Cl^- removal was investigated at 30°C, dosage of 1 g/L, Cl^- concentration of 100 mg/L and pH = 7.0. As shown in Fig. 3a, the Cl^- adsorption capacity of CaMnFe-LDHs increased rapidly from 88.40 to 140.05 mg/g during 10~240 min. And then, the Cl^- adsorption capacity increased slowly to 145.15 mg/g during 240~600 min. In the initial stage of adsorption, the adsorption amount increased rapidly due to the presence of a large number of unused adsorption sites on the adsorbent surface [16].

To further research the Cl^- adsorption process on CaMnFe-LDHs, the experimental data were fitted and analyzed using the pseudo-first-order model [Eq. (3)], the

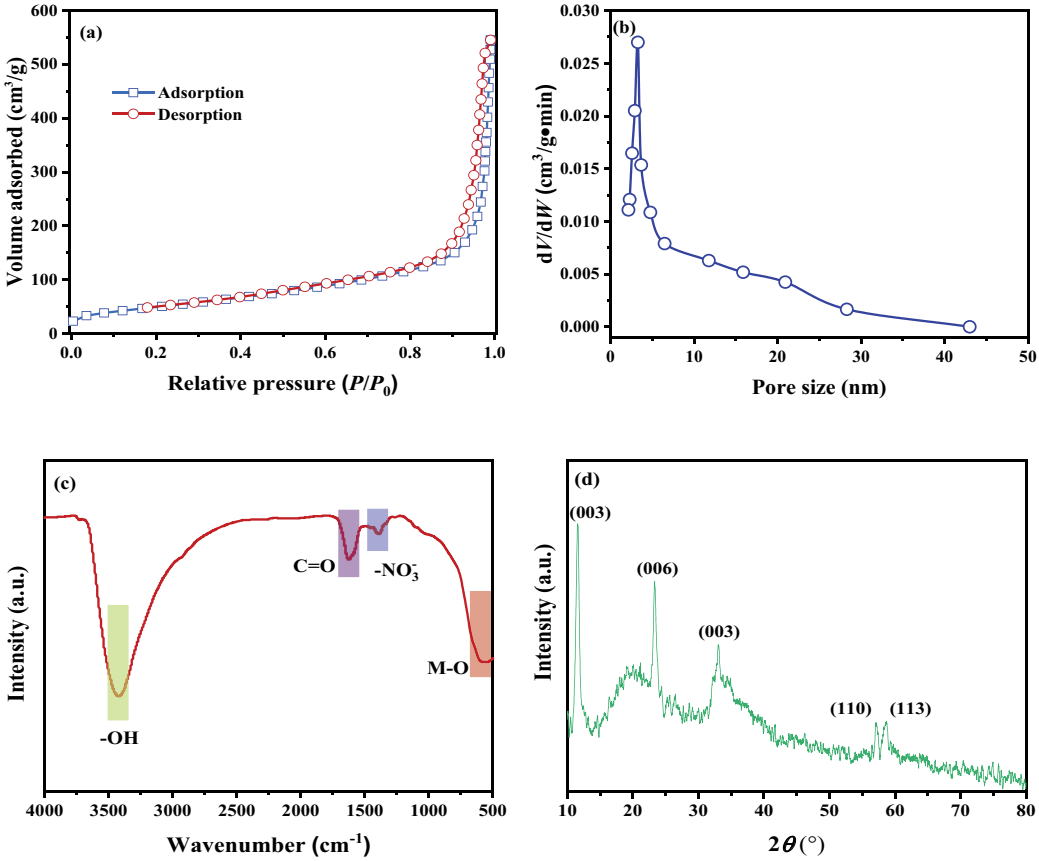

Fig. 2. N_2 adsorption–desorption (a), pore-size distribution (b), FTIR (c) and XRD (d) of CaMnFe-LDHs.

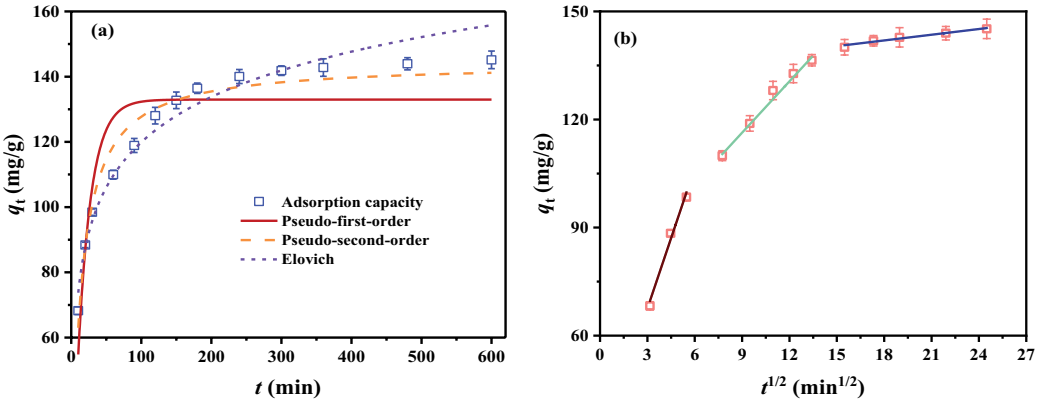

Fig. 3. Adsorption kinetics model (a) and intraparticle diffusion model (b) of Cl^- removal by CaMnFe-LDHs.

pseudo-second-order model [Eq. (4)], the Elovich model (Eq. 5) and the intraparticle diffusion model [Eq. (6)], and the results are shown in Fig. 4 and Table 1.

$$q_t = q_e\left(1 - e^{-k_1 t}\right) \tag{3}$$

$$q_t = \frac{q_e^2 k_2 t}{1 + q_e k_2 t} \tag{4}$$

$$q_t = \frac{1}{\beta}\ln\left(\alpha\beta t\right) \tag{5}$$

$$q_t = K_d t^{1/2} + C_i \tag{6}$$

where q_e and q_t are the adsorption capacity at adsorption equilibrium and at time "t", respectively, mg/g; k_1 (min^{-1}) and k_2 (g/mg min) are adsorption rate constant of the

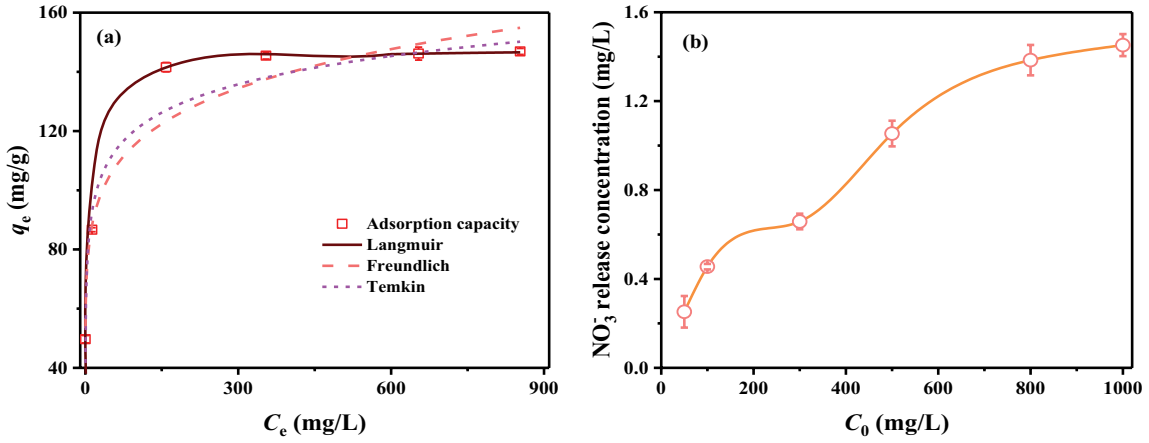

Fig. 4. Isothermal adsorption model (a) and release amount of NO_3^- concentration in solution after adsorption equilibrium (b).

Table 1
The kinetic model fitting parameters

Pseudo-first-order model			Pseudo-second-order model			Elovich model		
q_e	k_1	R^2	q_e	k_2	R^2	α	β	R^2
128.01	0.053	0.863	144.01	0.52×10^{-3}	0.984	76.00	0.049	0.979
Intraparticle diffusion model								
k_1	C_1	R_1^2	k_2	C_2	R_2^2	k_3	C_3	R_2^3
13.00	28.00	0.991	4.75	72.00	0.996	0.50	128.01	0.979

pseudo-first-order and the pseudo-second-order, respectively; α (mg/g min) and β are the initial absorbance and desorption constant, respectively; K_d (mg/m min$^{1/2}$) is the intraparticle diffusion constant; C_i is the boundary layer constant.

As shown in Table 1, the correlation coefficient (R^2) of pseudo-second-order model (R^2 = 0.984) was higher than those of pseudo-first-order model (R^2 = 0.863) and Elovich model (R^2 = 0.979), indicating that the pseudo-second-order model can more accurately describe the Cl^- adsorption process on CaMnFe-LDHs [16,33,34]. Moreover, this result suggested that the adsorption process belonged to chemisorption [14,16]. As shown in Fig. 4b, the intraparticle diffusion model divided the adsorption process into 3 stages. The first stage was the Cl^- diffusion from the liquid to the surface of the adsorbent. The second adsorption stage was the Cl^- diffusion from the surface to the pores, and the third stage was the Cl^- diffusion on the inner surface of the adsorbent until the adsorption equilibrium. Additionally, the intraparticle diffusion constants $K_{d1} > K_{d2} > K_{d3}$ and the boundary layer constants $C_1 < C_2 < C_3$ indicated that the first diffusion stage dominated the adsorption process [23].

The adsorption kinetic model shows that the pseudo-second-order model can better describe the process of Cl^- adsorption by CaMnFe-LDHs. In addition, the intraparticle diffusion model illustrates the different stages of Cl^- adsorption on CaMnFe-LDHs.

3.3. Adsorption isotherm

The effect of the initial concentration (50~1,000 mg/L) on the Cl^- removal was investigated at pH 7.0, a dosage of 1 g/L and 600 min. As shown in Fig. 4, the Cl^- adsorption capacity of CaMnFe-LDHs first increased and then reached stability. The experimental data were fitted and analyzed by Langmuir model [Eq. (7)], Freundlich model [Eq. (8)] and Temkin model [Eq. (9)].

$$q_e = \frac{q_{\max} K_b C_e}{1 + K_b C_e} \tag{7}$$

$$q_e = K_f C_e^{1/n} \tag{8}$$

$$q_e = \frac{RT}{b_T} \ln\left(A_T C_e\right) \tag{9}$$

where q_e (mg/g) is the adsorption capacity at equilibrium, mg/g; C_e (mg/L) is the Cl^- concentration at adsorption equilibrium; $q_{\max}$ (mg/g) and K_b (L/mg) are the theoretical maximum adsorption capacity and Langmuir equilibrium constant, respectively; K_f (mg^{1-n} L^n/g) and n are the Freundlich equilibrium constant and dimensionless number, respectively; A_T (1/g) and b_T (kJ/mol) are Temkin constants;

R is the global constant of gases (8.314 kJ/mol), and T is the absolute temperature (K).

As shown in Table 2, the correlation coefficients $R^2 > 0.9$ for the three models, but the Langmuir model had a higher correlation coefficient, which indicated that the Langmuir model was more consistent with the Cl^- adsorption on CaMnFe-LDHs. And then, this result reflected that the adsorption process was homogeneous and monolayer adsorption [16,26,27]. In addition, $1/n$ was less than 1 which represented that the adsorption process was easy to proceed and chemisorption occurs [33]. The maximum adsorption capacity (q_{max}) was 144.01 mg/g at 30°C through Langmuir model. Additionally, the NO_3^- concentration (Fig. 4b) in the solution increased with the initial Cl^- concentration, which indicated that ion exchange occurred during the Cl^- adsorption by CaMnFe-LDHs. That was, the NO_3^- between the CaMnFe-LDHs layers underwent ion exchange with Cl^- in the aqueous solution, which caused the NO_3^- in the solution to increase with the increase in the Cl^- concentration.

Table 2
Fitting parameters of adsorption isotherm

Langmuir model			Freundlich model			Temkin model		
q_{max}	K_L	R^2	K_f	n	R^2	b_T	A_T	R^2
144.01	0.11	0.982	62.00	7.25	0.958	186.60	13.50	0.979

3.4. Effects of environmental factors on the Cl^- adsorption

3.4.1. Dosage

In general, an increase in the amount of adsorbent dosage usually led to an increase in the adsorbent removal efficiency and a corresponding decrease in the adsorption capacity of the adsorbent. The effect of dosage (0.1~3.0 g/L) on the Cl^- adsorption process was investigated, as shown in Fig. 5a. The adsorption capacity decreased gradually with the increase of adsorbent dosage. Correspondingly, the Cl^- removal efficiency initially increased rapidly with increasing dosage. In essence, the effect of adsorbent dosage was due to the increase in the number of adsorption sites [16]. However, when the adsorption dosage exceeded 1 g/L, the removal efficiency increased very little. This may be due to the fact that excessive adsorbent dosage intensified the birdnesting between adsorbent particles,

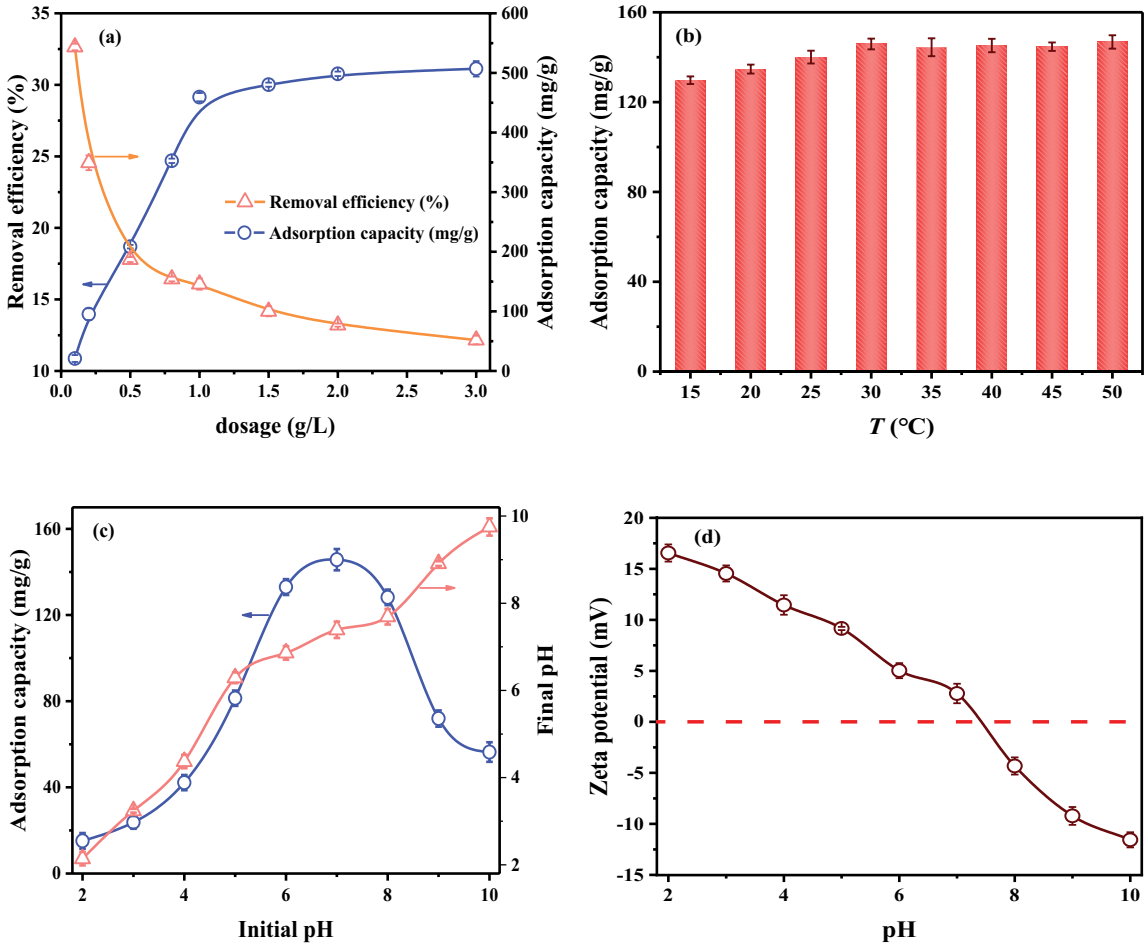

Fig. 5. Effects of dosage (a), adsorption temperature (b), and initial pH (c) of the solution on the Cl^- removal by CaMnFe-LDHs. Zeta potential of CaMnFe-LDHs at different pH (d).

which led to a decrease in the specific surface area of adsorbent [35]. Therefore, 1 g/L was considered as the most suitable adsorbent dosage in this study.

3.4.2. Adsorption temperature

In this study, the effect of adsorption temperature (15°C~50°C) on Cl^- adsorption was investigated, and the results were shown in Fig. 5b. As shown in Fig. 5b, the adsorption capacity increased with temperature as the temperature increased from 15°C to 30°C, and the adsorption capacity reached 145.90 mg/g at 30°C. When the temperature exceeded 30°C, there was little change in the Cl^- adsorption capacity of CaMnFe-LDHs. Therefore, 30°C was chosen as the optimum adsorption temperature for all the experiments.

3.4.3. Initial pH of the solution

Solution pH is an important influential parameter in the adsorption process, which can affect the charged nature of the adsorbent surface. The result of the initial pH on the Cl^- adsorption by CaMnFe-LDHs is shown in Fig. 5c. The Cl^- adsorption capacity gradually increased in the pH range of 2~7. The Cl^- adsorption capacity on CaMnFe-LDHs reached a maximum value of 145.70 mg/g at pH = 7.0. When pH > 7.0, the adsorption capacity sharply decreased to 56.40 mg/g. The zero potential point (pH_{pzc}) of the CaMnFe-LDHs was 7.39 (Fig. 5d). The solution pH was lower than 7.39, the H^+ in the solution occupied the O-containing function groups on the surface of CaMnFe-LDHs, which caused the adsorbent to protonate and positively charged, and the Cl^- adsorption capacity was enhanced [16,19]. When the solution pH was higher than 7.39, the O-containing function groups on the adsorbent surface deprotonated and turned to weaken the Cl^- adsorption [27]. However, this phenomenon caused a decrease in the Cl^- adsorption at pH > 7. Meanwhile, the complexes were formed between Cl^- and CaMnFe-LDHs and H^+ was released at this process, which caused a decrease in the solution pH.

3.5. Adsorption mechanism

FTIR analysis of CaMnFe-LDHs before and after Cl^- adsorption is shown in Fig. 6a. The FTIR spectra before and after adsorption did not change greatly, which indicated that CaMnFe-LDHs had good stability. The –OH group in the CaMnFe-LDHs was shifted. In addition, the C=O group shifted to 1,625 cm^{-1} and showed a decrease in intensity. Similarly, the M–O group was also shifted after adsorption. The above results suggested that O-containing groups in CaMnFe-LDHs were involved in the Cl^- adsorption [18,33]. Notably, the NO_3^- group showed a weakening after adsorption, presumably due to the ionic exchange of NO_3^- with Cl^- in the CaMnFe-LDHs [19].

The XRD analysis of the CaMnFe-LDHs before and after the Cl^- adsorption is shown in Fig. 6a. After the adsorption, the diffraction peaks of the CaMnFe-LDHs all appeared to be weakened. This phenomenon was presumed to be an ion exchange between NO_3^- in the CaMnFe-LDHs and Cl^-, resulting in a weakening of the diffraction peaks of the LDHs [16]. The results of the above analysis suggested that the mechanism of Cl^- removal by CaMnFe-LDHs involved adsorption of O-containing groups and ion exchange.

3.6. Solidification performance of CaMnFe-LDHs in cement slurry block

The effects of admixture ratios (0:100, 5:100, 10:100, 15:100, 20:100 and 25:100) and curing age (3, 7 and 27 d) on the Cl^- solidification were investigated after the immersion of 28 d (Fig. 7a). A small amount of Cl^- was still cured when CaMnFe-LDHs was not mixed. On the one hand, the reason for this was mainly the chemical combination of chloride ions with the cement slurry block to generate Friedel's salt [6,28]. On the other hand, Cl^- were physically adsorbed by the cement hydration product C–S–H gel [23,29]. From the data of EG, the amount of Cl^- solidification increased with the admixture ratio increase, and there was no obvious slowing down trend in the growth rate. Notably, the Cl^- adsorption capacity of cement slurry block also increased significantly and gradually with the admixture ratio increase. When the admixture ratio of CaMnFe-LDHs in cement slurry block was 25:100, the amount of Cl^- solidification was about 155.74 mg and the adsorption capacity was 56.15 mg/g. Additionally, the solidification amount and adsorption capacity of Cl^- gradually increased with the increase of curing age. The cement slurry block was always in the Cl^- solution, and the water inside the cement

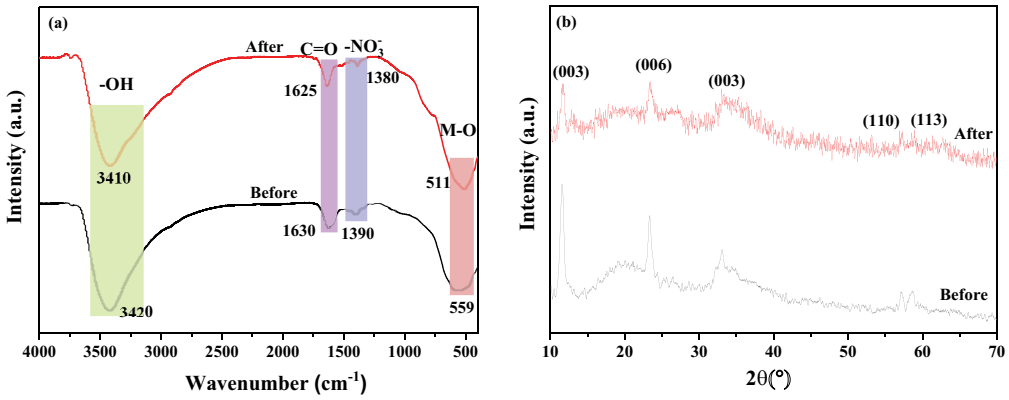

Fig. 6. FTIR (a) and XRD (b) of adsorbent before and after Cl^- adsorption.

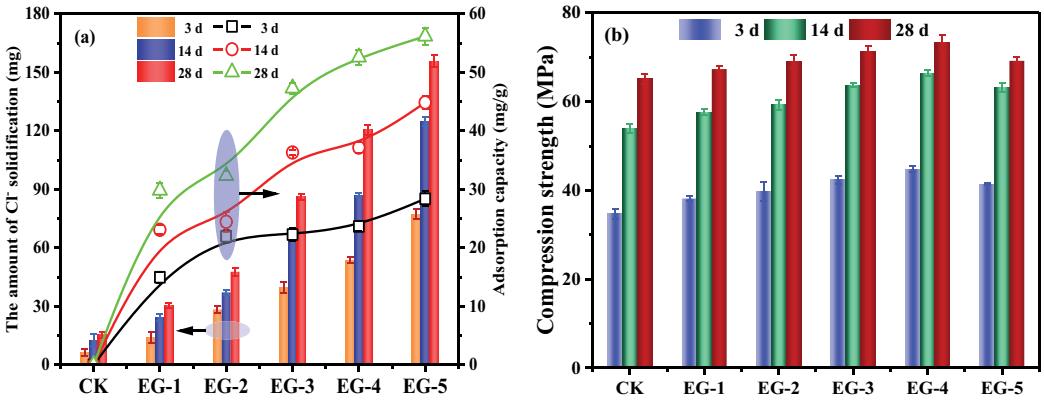

Fig. 7. The Cl^- curing ability (a) and compressive strength (b) of cement slurry block with different CaMnFe-LDHs admixtures.

slurry block was in a dynamic exchange process with the water in the external environment [4]. Due to the potential difference, Cl^- continuously invaded the cement slurry and transferred to its interior.

The compressive strength of the cement slurry block with different admixture ratios was tested and the result is shown in Fig. 7b. The compressive strength of the EG groups with CaMnFe-LDHs was higher than that of the CK group. With the increase of curing age, the compressive strength of the each group increased slowly. The compressive strength growth was especially obvious at 3 and 7 d, which can be inferred that CaMnFe-LDHs played the role of accelerating the hydration of cement. The compressive strength increased with the increase of admixture, while the compressive strength of EG-5 decreased. This result indicated that the admixture of CaMnFe-LDHs did not lead to a linear increase of the compressive strength, while there was an optimal admixture point. The enhancement of compressive strength may be that the CaMnFe-LDHs accelerated the crystallization rate of hydration products in cement slurry block [25]. The effect of CaMnFe-LDHs was like that of calcium nitrate in that the nitrate can assist the release of hydroxide from cement clinker particles, which in turn increased the dissolution rate of silicate and thus accelerated the generation of C–S–H in cement slurry block [17,20,29,32]. Therefore, the cement slurry block had a better ability to cure Cl^- at a admixture ratio of 20:100.

4. Conclusion

CaMnFe-LDHs were successfully prepared by co-precipitation method. The Cl^- adsorption process on CaMnFe-LDHs was in accordance with the pseudo-second-order model and Langmuir model. The Cl^- maximum adsorption of CaMnFe-LDHs could reach 144.01 mg/g. The mechanism of Cl^- removal by CaMnFe-LDHs involved adsorption of O-containing groups and ion exchange. Solidification experiments showed that the cement slurry block with CaMnFe-LDHs had significantly improved its Cl^- solidification ability compared to ordinary cement slurry block. The results indicated that CaMnFe-LDHs incorporation can effectively prevent the attack of Cl^- on the cement slurry block.

Funding

This work was supported by Key Projects of Scientific Research of Xi'an Traffic Engineering Institute (2021KY-22).

Conflicts of interest

The authors declare that we have no competing financial interests.

References

[1] Y. Yang, K.H. Tan, Y.H. Qin, Review of research on the influencing factors of chloride ion diffusion in concrete, Mater. Rep., 35 (2021) 13109–13118.
[2] Z.G. Li, W.J. Ji, Y. Li, J.P. Liu, Research progress on application of layered double hydroxides in cement concrete, Concrete, 1 (2021) 25–30.
[3] Y.Y. Zhu, J. Geng, D. Li, Recent research and hotspot analysis of corrosion inhibition of reinforcing steel in concrete by Mg-Al CLDHs, Concrete, 9 (2019) 21–24.
[4] Y. Chen, Z. Shui, C. Wei, G. Chen, Chloride binding of synthetic Ca–Al–NO_3 LDHs in hardened cement paste, Construct. Build. Mater., 93 (2015) 1051–1058.
[5] L. Chi, Z. Wang, Y.F. Zhou, S. Lu, Y. Yao, Layered double hydroxides precursor as chloride inhibitor: synthesis, characterization, assessment of chloride adsorption performance, Materials, 11 (2018) 2537, doi: 10.3390/ma11122537.
[6] P. Duan, Z.H. Shui, G.W. Chen, Influence of LDHs on chloride ion binding in cementitious materials, Key Eng. Mater., 599 (2014) 34–38.
[7] J.T. Ma, D.G. Wang, P. Duan, Y.K. Shi, Sulfate ions immobilization of calcined layered double hydroxides in hardened cement paste and concrete, J. Wuhan Univ. Technol., 34 (2019) 1400–1407.
[8] Z.F. Ren, J. He, C.Q. Zhang, X. Duan, Removal of chloride anion by calcined layered double hydroxides, Fine Chem., 19 (2002) 339–342.
[9] E. Asgari, A. Sheikhmohammadi, J. Yeganeh, Application of the Fe_3O_4-chitosan nano-adsorbent for the adsorption of metronidazole from wastewater: optimization, kinetic, thermodynamic and equilibrium studies, Int. J. Biol. Macromol., 164 (2020) 694–706.
[10] H. Godini, F. Hashemi, L. Mansuri, M. Sardar, G. Hassani, S.M. Mohseni, A.A. Alinejad, S. Golmohammadi, A. Sheikh Mohammadi, Water polishing of phenol by walnut green hull as adsorbent: an insight of adsorption isotherm and kinetic, J. Water Reuse Desal., 6 (2016) 544–552.
[11] Y. Li, T.C. Wang, S.S. Zhang, Y.L. Zhang, L.L. Yu, R.J. Liu, Adsorption and electrochemical behavior investigation of methyl blue onto magnetic nickel-magnesium ferrites prepared

via the rapid combustion process, J. Alloys Compd., 885 (2021) 160969, doi: 10.1016/j.jallcom.2021.160969.
[12] A. Sheikhmohammadi, S.M. Mohseni, B. Hashemzadeh, E. Asgari, M. Almasiane, Fabrication of magnetic graphene oxide nanocomposites functionalized with a novel chelating ligand for the removal of Cr(VI): modeling, optimization, and adsorption studies, Desal. Water Treat., 160 (2019) 297–307.
[13] A.S. Mohammadi, M. Sardar, M. Almasian, Equilibrum and kinetic studies on the adsorption of Penicillin G by chestnut shell, Environ. Eng. Manage. J., 15 (2016) 167–173.
[14] Q. Xu, Y.Y. Xu, J.M. Xue, F.H. Zhu, Z.P. Zhong, R.J. Liu, An innovative alcohol-solution combustion-calcination process for the fabrication of $NiFe_2O_4$ nanorods and their adsorption characteristics of methyl blue in aqueous solution, Mater. Res. Express, 8 (2021) 095003, doi: 10.1088/2053-1591/ac1ecd.
[15] N. Tang, W.F. Cen, M.Y. Zhao, L.M. Wu, J. Wang, Chloride ions binding of calcium-aluminum hydrotalcite in cementitious material, J. Shenyang Jianzhu Univ. (Nat. Sci.), 37 (2021) 900–906.
[16] S. Yoon, J. Moon, S. Bae, X.N. Duan, E.P. Giannelis, P.M. Monteiro, Chloride adsorption by calcined layered double hydroxides inhardened Portland cement paste, Mater. Chem. Phys., 145 (2014) 376–386.
[17] J.T. Ma, L. Chen, W. Chen, K. Wang, Research on the combination of LDHs and MK on improving the chloride ion resistance of concrete, J. Wuhan Univ. Technol., 35 (2013) 34–39.
[18] J.K. Guo, Z. Zhou, F.Y. Peng, X.S. Bai, Preparation of CNTs/MgAl-LDHs composites and their adsorption properties for chloride ions, Mater. Sci. Forum, 956 (2019) 305–313.
[19] G.J. Ke, L. Zhang, P.F. Yang, H.D. Zhao, H.J. Tan, Controlled synthesis of Mg-Al hydrotalcites with different morphologies and their adsorption performances for chloride ion, Fine Chem., 34 (2017) 1107–1113.
[20] G.F. Peng, N.Q. Feng, Q.M. Song, Influence of chloride-ion adsorption agent on chloride ions in concrete and mortar, Materials, 7 (2014) 3415–3426.
[21] D.D. Wang, Q. Zhu, Y.Y. Su, J. Li, A.W. Wang, Z.P. Xing, Preparation of MgAlFe-LDHs as a deicer corrosion inhibitor to reduce corrosion of chloride ions in deicing salts, Ecotoxicol. Environ. Saf., 174 (2019) 164–174.
[22] R.T. Yin, S.S. Zhang, Y.Y. Xu, J.M. Xue, J.Q. Bi, R.J. Liu, Adsorption mechanism and electrochemical properties of methyl blue onto magnetic $Co_xCu_{(1-x)}Fe_2O_4$ nanoparticles prepared via an alcohol solution of nitrate combustion and calcination process, J. Inorg. Organomet. Polym. Mater., 31 (2021) 3584–3594.
[23] L. Yang, J.B. Xu, Y.B. Huang, L.B. Li, Using layered double hydroxides and anion exchange resin to improve the mechanical properties and chloride binding capacity of cement mortars, Construct. Build. Mater., 272 (2021) 122002, doi: 10.1016/j.conbuildmat.2020.122002.
[24] X.G. Yang, B.S. Jin, L.L. Yu, F.H. Zhu, Y.Y. Xu, R.J. Liu, Preparation and characterization of magnetic α-Fe_2O_3/Fe_3O_4 heteroplasmon nanorods via the ethanol solution combustion process of ferric nitrate, Materials Research Express, 8 (2021) 025011.
[25] B. Wu, J.D. Zuo, B.Q. Dong, F. Xing, C.Y. Luo, Study on the affinity sequence between inhibitor ions and chloride ions in Mg–Al layer double hydroxides and their effects on corrosion protection for carbon steel, Appl. Clay Sci., 180 (2019) 105181, doi: 10.1016/j.clay.2019.105181.
[26] J.X. Xu, Q.P. Tan, L.H. Jiang, Y.J. Mei, Influence of SO_4^{2-} on adsorption of Cl^- and rust resistance of MgAl-LDHs, J. Southeast Univ., 49 (2019) 507–513.
[27] Y.J. Mei, J.X. Xu, L.H. Jiang, P. Chen, Q.P. Tan, Protecting of steel form chloride-induced corrosion by cement slurry coatings with calcined Mg-Al layered double hydroxide, Mater. Rep., 32 (2018) 3941–3947.
[28] Y.Z. Chen, W.S. Yin, T. Sun, C.H. Shen, Y.F. Wang, J.X. Xu, Effect of high addition of SCMs on the capacity of cement-based materials binding chloride ions, Bull. Chin. Ceram. Soc., 35 (2016) 1664–1668.
[29] Y. Ma, J. Geng, D. Li, Influence of calcined hydrotalcite on chloride penetration in mortar, Bull. Chin. Ceram. Soc., 37 (2018) 1195–1198.
[30] J. Hu, L. Lv, Researches on the removal capacity of chloride ions from aqueous solution by calcined Mg–Al-CO_3 LDH, Ind. Water Treat., 28 (2008) 59–61.
[31] B.L. Lei, Y. Zhang, L.H. Zhang, Structural characterization of nano hydrotalcite and its adosption performance for chloride ion, Mater. Rep., 29 (2015) 64–67.
[32] A.G. Wang, B.C. L, P. Duan, Y.Y. Wu, K. Liu, Improved chloride ion penetration resistance of geopolymer by adding calcined layered double hydroxides, Mater. Rev., 32 (2018) 1707–1710.
[33] J.F. Wei, J.X. Xu, Y.J. Mei, Q.P. Tan, Chloride adsorption on aminobenzoate intercalated layered double hydroxides: kinetic, thermodynamic and equilibrium studies, Appl. Clay Sci., 187 (2020) 105495, doi: 10.1016/j.clay.2020.105495.
[34] S. Pan, Q.M. Yu, L.L. Yu, Y.Y. Xu, R.J. Liu, Preparation and antimicrobial performance of $Ni_{0.5}Zn_{0.5}Fe_2O_4$@Ag nanocomposites, J. Inorg. Organomet. Polym. Mater., 31 (2021) 875–885.
[35] W.Y. Zhang, Y. Liu, L.J. Xi, W.H. Zhang, Study on removal performance of chlorine ion from wastewater with clinoptilolite supported Mg-Al-Fe hydrotalcite, Bull. Chin. Ceram. Soc., 32 (2013) 2481–2484.